

# Effects of system-bath coupling on Photosynthetic heat engine: A polaron master equation approach

M. Qin<sup>1,2</sup>, H. Z. Shen<sup>1</sup>, X. L. Zhao<sup>1,2</sup>, and X. X. Yi<sup>1</sup> \*

<sup>1</sup>*Center for Quantum Sciences and School of Physics,  
Northeast Normal University, Changchun 130024, China*

<sup>2</sup>*School of Physics and Optoelectronic Technology  
Dalian University of Technology, Dalian 116024, China*

In photosynthesis, the fundamental principles responsible for the near-unit quantum efficiency of the conversion of solar to chemical energy remains unknown. Under natural conditions, the formation of stable charge separation states in bacteria and plant reaction centers is strongly affected by the coupling of electronic degrees of freedom to a wide range of vibrational motions. These inspire and motivate us to explore the effects of environment on the operation of such complexes. In this paper, we apply the polaron master equation, which offers the possibilities to interpolate between weak and strong system-bath coupling, to study how system-bath couplings affect charge transfer processes in Photosystem II reaction center (PSII RC) inspired quantum heat engine (QHE) model in a wide parameter range. The effects of bath correlation and temperature, together with the combined effects of these factors are also discussed in details. The results show a variety of dynamical behaviours. We interpret these results in terms of noise-assisted transport effect and dynamical localization which correspond to two mechanisms underpinning the transfer process in photosynthetic complexes: One is resonance energy transfer and the other is dynamical localization effect captured by the polaron master equation. The effects of system-bath coupling and bath correlation are incorporated in the effective system-bath coupling strength determining whether noise-assisted transport effect or dynamical localization dominates the dynamics and temperature modulates the balance of the two mechanisms. Furthermore, these two mechanisms can be attributed to one physical origin: bath-induced fluctuations. The two mechanisms is manifestations of dual role played by bath-induced fluctuations within respective parameter range. In addition, we find that the effective voltage of QHE exhibits superior robustness with respect to the bath noise as long as the system-coupling strength is not too large.

PACS numbers: 42.50.Gy, 42.50.Nn, 84.60.Jt, 82.39.Jn

## I. INTRODUCTION

In the photosynthesis process of plants and bacteria, the sun's energy is captured and stored by a series of events that convert the pure energy of light into the biochemical energy needed to power life, providing all our food and most of our energy resources [1, 2]. After absorption of a photon, an excited state on a pigment molecule is created. The excitation is transferred efficiently through antenna system until it arrives at a reaction center (RC) where charge separation and conversion of pure energy of excited states to chemical changes take place [3, 4]. Numerous studies focus on the precise mechanisms underlying the high efficiency transport [5–8]. Recent experimental demonstrations of oscillatory electronic dynamics in photosynthetic system have raised the quantum coherent dynamics may be relevant in photosynthetic energy transfer of living organisms in conditions that are often defined as hot and wet [9–16]. This causes much debate whether quantum coherence promotes the efficiency and the role of environment on energy transfer are also extensively discussed [17–30]. Therefore, understanding the underlying mechanism of such highly efficient excitation energy transduction in natural photosynthetic system can assist us in improving the design of promising artificial structures for quantum transport and optimized light-harvesting devices [31–34].

Exposed to sunlight, RC complexes operate as Nature's so-

lar cells with very high yield for light-to-charge conversion. Charge separation in RCs has been a question of recent studies. Dorfman et al have introduced a promising approach in which the photosynthetic reaction center is viewed as a quantum heat engine (QHE), and showed that attributed to noise-induced quantum coherence, the photocurrent of the photocell based on Photosystem II reaction center (PSII RC) can be increased by 27% compared to an equivalent classical photocell [35]. Ref. [36] investigates the effects of structured environment on electron transfer in PSII RC-based photocell devices placed between two electrodes. In experiment, steady-state and multi-dimensional optical spectroscopy have revealed that the process of excitation energy transfer and conversion to stable charge separated states is strongly affected by the interaction between excitonic or electronic degrees of freedom to a wide range of vibrational modes of surrounding bath [37–39]. In spite of these theoretical and experimental efforts, the fundamental principles responsible for charge transfer in PSII reaction center are still indistinct and under scrutiny. These motivate us to consider the effect of system-bath coupling on charge transfer processes in PSII RC.

Traditionally, transfer processes in open system has been described by Förster-Dexter theory [40, 41] if the electronic coupling between chromophores is very weak compared with their interaction with bath. When the electronic coupling is strong and the system-bath coupling is weak, it is necessary to consider relaxation between delocalized exciton states. In this limit, excitation energy transfer (EET) dynamics are described by the coupled Redfield equations [42, 43]. However, for the intermediate coupling regime where the energy scales

---

\*Corresponding address: yixx@nenu.edu.cn

of electronic coupling and exciton-bath interaction are comparable, both Förster-Dexter and Redfield theory become invalid since a proper perturbative term in theoretical treatment does not exist. In spite of the invalidity for the intermediate coupling case, these two second-order perturbative theories also have a problem of being not precise enough according to recent spectroscopic experiments on photosynthetic complexes [10, 12, 13]. This calls for non-perturbative techniques to obtain numerically exact dynamics, for example, the quasi-adiabatic propagator path integral (QUAPI) [44, 45], the hierarchy equations of motion (HEOM) [46, 47] and the multiconfiguration time-dependent Hartree approach [48–50]. Nevertheless, these methods are computationally sophisticated and not trivial to implement especially for large system size or multi-excitation case. Thus, a computationally economical and an appropriate qualitative and quantitative account of dynamics for the intermediate case is in urgent need.

Recently, a polaron transformed second-order master equation has been developed to treat coherent energy transfer in molecular system [51–67]. Despite perturbative, this approach allows for a consistent exploration of the intermediate regime in which many multichromophoric systems operate, serving as a bridge between the Redfield and Förster-Dexter theories. In this formalism, the system-plus-phonon bath Hamiltonian is transformed into the polaron frame, in which the system Hamiltonian is dressed by a phonon and electronic couplings are renormalized and fluctuate due to coupling with phonon bath. Then the transformed system-bath interaction term can be treated as a perturbation and the master equation can be obtained using standard projection operator techniques. This approach combines the excitation with its surrounding bath as an entity instead of considering the exciton and bath separately and has been reliably applied to describe EET in light-harvesting complexes in the intermediate coupling regime as a quantitative method. In this paper, we apply this approach to shed light on the question how system-bath couplings affect charge transfer processes in PS II RCs in a wide parameter range.

The remainder of the paper is organized as follows: In Sec. II, we introduce a model of PSII RC-based quantum heat engine to describe the charge separation. Then we review the formalism of polaron transformation and give polaron master equation for our model. The concepts of effective voltage and power generated applied for assessing the performance of our QHE system is also introduced in this section. In Sec. III, we first elucidate the temperature and system-bath coupling strength dependence of the effective coupling and its effect on the equilibrium structure of the exciton-ICTS system, and then focus on the separate effects of system-bath coupling  $\gamma$ , cross-correlation coefficient  $c$  and temperature  $T$ , respectively. Furthermore we discuss the combined effects of these parameters on the current and power generated by QHE system in details. We utilize Franck-Condon factor and the concept of effective system-bath coupling including the effects of both individual system-bath coupling and bath correlation to explain the various behaviours of QHE performance. Two mechanisms dominating the transfer dynamics are concluded. In addition, we explore the effective voltage of QHE model subjected to bath

noise. Sec. IV is devoted to concluding remarks. We leave the detailed derivation of polaron master equation in the appendix.

## II. THEORY

### A. Model system

We first illustrate the structure of PSII RC complex in Fig. 1 (a). PSII RC contains four chlorophylls (special pair  $P_{D1}$  and  $P_{D2}$  and accessory  $Chl_{D1}$  and  $Chl_{D2}$ ) and two pheophytins ( $Phe_{D1}$  and  $Phe_{D1}$ ) arranged in two branches ( $D_1$  and  $D_2$ ). Only  $D_1$  branch takes an active part in the electron transfer process. Although two different excited states ( $P_{D1}P_{D2}Chl_{D1}$ )\* and  $(Chl_{D1}Phe_{D1})^*$  are discovered to initiate charge separation via  $Chl_{D1}$  and  $P_{D1}$  pathways respectively, we focus on the  $Chl_{D1}$  pathway, since experimental spectroscopy and theoretical researches reveals that charge transfer is mostly initiated from  $(Chl_{D1}Phe_{D1})^*$  [68]. As shown in Fig. 1 (b),  $Chl_{D1}$  rapidly loses an electron to  $Phe_{D1}$ , generating an initial charge transfer state (ICTS)  $|Chl_{D1}^+ Phe_{D1}^- \rangle$ . Then the positive and negative charges are spatially separated to produce a secondary charge transfer state  $|P_{D1}^+ Phe_{D1}^- \rangle$  which leads to energy stabilization. Then the electron is released from the system to drive a chain of chemical reactions including the reduction of NADP to NADPH, the synthesis of ATP and the oxidized part of the RC splits water, releasing molecular oxygen, and the system is positively charged denoted by  $P_{D1}^+ Phe_{D1}$ . At last, the system captures an electron from their surroundings to complete the cycle and returns to the ground state in which none of the six pigment molecules are excited.

The biologically inspired quantum heat engine (QHE) transforms high-energy thermal photon radiation into low-entropy electron flux. In Fig. 2, we analyse the photosynthetic reaction center as a five-level scheme which models the photon absorption and charge separation events described above, using the following states: the ground state  $|0\rangle$ , the exciton state  $|(Chl_{D1}Phe_{D1})^*\rangle \equiv |1\rangle$ , the ICTS  $|Chl_{D1}^+ Phe_{D1}^- \rangle \equiv |2\rangle$ , the secondary charge transfer state  $|P_{D1}^+ Phe_{D1}^- \rangle \equiv |\alpha\rangle$  and the positively charged state  $|P_{D1}^+ Phe_{D1}\rangle \equiv |\beta\rangle$ . After absorption of a solar photon, the system is promoted from the ground state  $|0\rangle$  to the exciton state  $|1\rangle$  with a rate  $\gamma_h$ . Then the primary charge separation takes place which channels energy to the ICTS  $|2\rangle$ . This process is subjected to a phonon bath LTB3 (the third low temperature phonon bath). Then follows the secondary charge separation in which the positive and negative charges are spatially separated. For simplicity, the secondary charge separation is treated as a dissipation transition from  $|2\rangle$  to the secondary charge transfer state  $|\alpha\rangle$  with excess energy radiated as a phonon into the phonon bath LTB1 (the first low temperature phonon bath) with a rate  $\gamma_{c1}$ . This is a phenomenological treatment without going into the details of actual parameters of PSII RC. Then the electron is released from the system to perform work with a relaxation rate  $\Gamma$ , resulting in a current from  $|\alpha\rangle$  to the positively charged state  $|\beta\rangle$  driving a chain of chemical reactions, leading eventually to the stable storage of

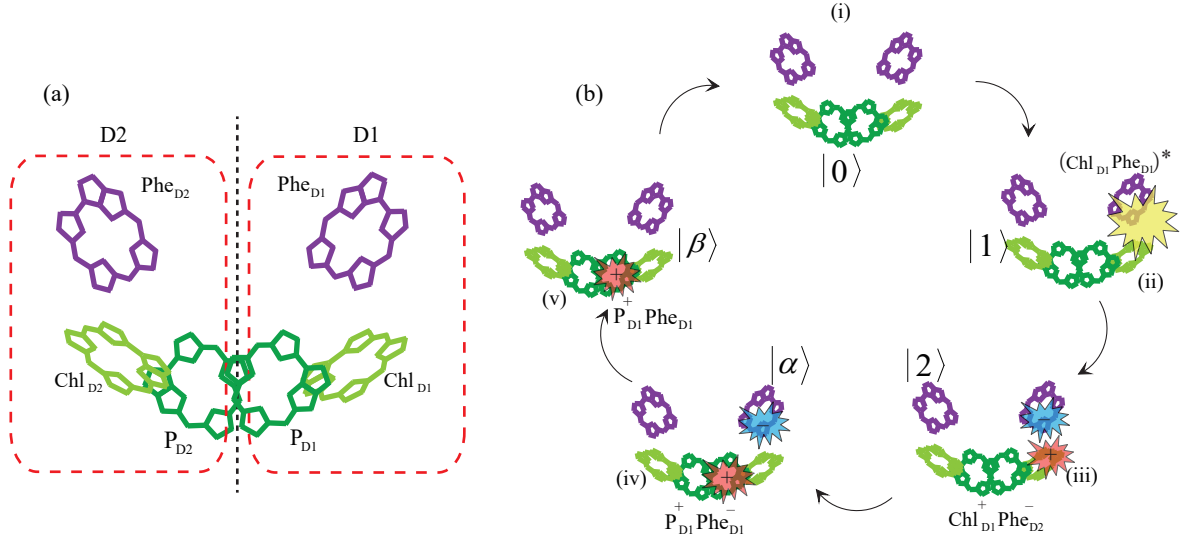


FIG. 1: (Color online) (a) Arrangement of six core-pigments in the PSII RC. It consists of a special pair  $\text{P}_{D1}$ ,  $\text{P}_{D2}$ , two accessory chlorophylls  $\text{Chl}_{D1}$ ,  $\text{Chl}_{D2}$ , and two pheophytins  $\text{Phe}_{D1}$ ,  $\text{Phe}_{D2}$ . (b) Charge transfer process in our QHE model. (i) The lowest energy configuration with all six pigments in neutral ground state after an electron has been replenished at the special pair. (ii) Excited state  $(\text{Chl}_{D1}\text{Phe}_{D1})^*$  after absorption of a photon. (iii) Primary charge transfer state  $\text{Chl}_{D1}^+\text{Phe}_{D1}^-$  after  $\text{Chl}_{D1}$  as the electron donor rapidly loses an electron to the nearby electron acceptor molecule  $\text{Phe}_{D1}$ . (iv) Secondary charge transfer state  $\text{P}_{D1}^+\text{Phe}_{D1}^-$  after the positive and negative charges are spatially separated. (v) Positively charged state  $\text{P}_{D1}^+\text{Phe}_{D1}$  after an electron has been released from the system to perform work.

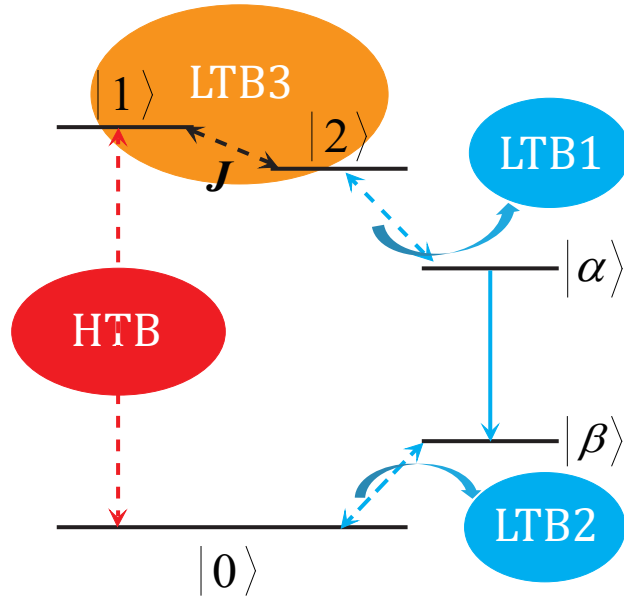


FIG. 2: (Color online) Schemes of the QHE model based on PSII RC. HTB denotes the high-temperature photon bath from sunlight, while LTB1, LTB2 and LTB3 stand for the low-temperature phonon baths attributed to molecular vibrational degrees of freedom. HTB induces transition from the ground state  $|0\rangle$  to the single-exciton states  $|1\rangle$ . The primary charge separation denoted by the transition between  $|1\rangle$  and  $|2\rangle$  with interpigment coupling  $J$  is subject to LTB3. LTB1 induces transition from  $|2\rangle$  to the secondary charge transfer state  $|\alpha\rangle$  with the excess energy radiated as a phonon, phenomenologically representing the secondary charge transfer process in which the positive and negative charges are spatially separated. Then the electron is released from state  $|\alpha\rangle$  resulting a current from  $|\alpha\rangle$  to  $|\beta\rangle$ . LTB2 induces transition from the positively charged state  $|\beta\rangle$  to the ground state  $|0\rangle$  which brings the electron back to the system with emission of a phonon with excess energy.

solar energy. The current is thus determined by the relaxation rate  $\Gamma$  and the population of  $|\alpha\rangle$ ,

$$j = e\Gamma\rho_{\alpha\alpha} \quad (1)$$

Finally, to complete the cycle, we assume another population transfer process to take place, emitting a phonon with excess energy into the phonon bath LTB2 (the second low temperature phonon bath), bringing the electron back to the neutral ground state  $|0\rangle$  with a rate  $\gamma_{c2}$ .

In this paper, we focus on the effects of LTB3 phonon modes on the charge transfer process of exciton-ICTS dimer system ( $|1\rangle$  and  $|2\rangle$ ) over a broad range. Thus the coupling of the exciton state  $|1\rangle$  and the ICTS  $|2\rangle$  with LTB3 will be considered rigorously. To describe energy transfer between  $|1\rangle$  and  $|2\rangle$ , we consider a Frenkel exciton model Hamiltonian in the single exciton manifold:

$$\begin{aligned} H &= H_s + H_b + H_{sb}, \\ H_s &= \sum_{m=1,2} \varepsilon_m |m\rangle \langle m| + J(|1\rangle \langle 2| + |2\rangle \langle 1|), \\ H_b &= \sum_k \omega_{vk} b_k^\dagger b_k, \\ H_{sb} &= \sum_{m=1,2} \sigma_m^+ \sigma_m^- \sum_k (g_{vk,m} b_k^\dagger + g_{vk,m}^* b_k), \end{aligned} \quad (2)$$

$H_s$  describes the Frenkel-exciton Hamiltonian where  $\varepsilon_m$  is the relative site energy of the exciton state  $|1\rangle$  and the ICTS  $|2\rangle$  with respect to the ground state  $|0\rangle$  whose energy is set to 0.  $J$  denotes the electronic coupling between states  $|1\rangle$  and  $|2\rangle$ .  $H_b$  represents the Hamiltonian of LTB3 with  $b_k^\dagger$  ( $b_k$ ) the creation/annihilation operator and  $\omega_{vk}$  the frequency of the  $k$ th phonon mode of LTB3.  $H_{sb}$  is the interaction Hamiltonian describing the coupling of the exciton state  $|1\rangle$  and the ICTS  $|2\rangle$  with the phonon bath LTB3, dominated by site energy fluctuations, with  $g_{vk,m}$  the coupling strength between the  $k$ th phonon mode and the  $m$ th state.

## B. Polaron transformation

The formulism of polaron transformation is first used to treat charge transfer in organic molecular crystals by Holstein and then developed by Silbey etc to consider population dynamics in EET. It assumes that the electronic excitation moves collectively with its surrounding bath deformation rather than separating the exciton and bath. Following Grover and Silbey [61], we move into the polaron frame defined by a unitary transformation  $\tilde{H} = e^S H e^{-S}$ , where  $S = \sum_{m=1,2} |m\rangle \langle m| \sum_k (g_{vk,m} b_k^\dagger - g_{vk,m}^* b_k) / \omega_{vk}$ . Within this trans-

formed frame, the renormalized Hamiltonian reads

$$\begin{aligned} \tilde{H} &= \tilde{H}_s + \tilde{H}_b + \tilde{H}_{sb}, \\ \tilde{H}_s &= \sum_{m=1,2} \tilde{\varepsilon}_m |m\rangle \langle m| + J\kappa(|1\rangle \langle 2| + |2\rangle \langle 1|), \\ \tilde{H}_b &= \sum_k \omega_{vk} b_k^\dagger b_k, \\ \tilde{H}_{sb} &= J(\tilde{B}|1\rangle \langle 2| + \tilde{B}^\dagger |2\rangle \langle 1|), \end{aligned} \quad (3)$$

where  $\tilde{\varepsilon}_m$  is the shifted on-site energy with the corresponding site-dependent reorganization energy  $\lambda_m = \sum_k \frac{|g_{vk,m}|^2}{\omega_{vk}}$ , such that  $\tilde{\varepsilon}_m = \varepsilon_m - \lambda_m$ .  $\tilde{B}$  signifies the shifted bath operator defined as  $\tilde{B} = B - \kappa$  with the bath operator  $B = e^{\sum_k (\delta g_{vk,12} b_k^\dagger - \delta g_{vk,12}^* b_k) / \omega_{vk}}$ . The factor  $\delta g_{vk,12} = g_{vk,1} - g_{vk,2}$  is the difference of system-bath couplings  $g_{vk,1}$  and  $g_{vk,2}$  in state  $|1\rangle$  and  $|2\rangle$ , respectively. Here, we define bath-induced renormalization factor as  $\kappa = \langle B \rangle$ . We see that, in the polaron theory, the electronic system-plus-phonon bath Hamiltonian is transformed into the polaron frame in which electronic couplings are renormalized and fluctuate due to the interaction with bath modes, while the free Hamiltonian of phonon bath LTB3 remains unchanged. In this formulism, the reorganization energy of the  $m$ th site can be calculated as

$$\lambda_m = \sum_k \frac{|g_{vk,m}|^2}{\omega_{vk}} = \int_0^\infty \frac{J_{mm}(\omega)}{\omega} d\omega, \quad (4)$$

We define an effective electronic couplings  $\tilde{J} = J\kappa$ , and the expectation value of the bath operator for a harmonic oscillator bath in thermal equilibrium evaluates to

$$\begin{aligned} \kappa = \langle B \rangle &= \text{Tr}[\rho'_b B] \\ &= \exp\left\{-\frac{1}{2} \int_0^\infty \frac{1}{\omega^2} [J_{11}(\omega) - 2J_{12}(\omega) \right. \\ &\quad \left. + J_{22}(\omega)] \coth\left(\frac{\beta\omega}{2}\right) d\omega\right\} \end{aligned} \quad (5)$$

where  $\beta = 1/k_B T$  is the inverse temperature and  $\rho'_b = \exp(-\beta \tilde{H}_b) / \text{Tr}[\exp(-\beta \tilde{H}_b)]$  denotes the thermal state of the phonon bath.  $\kappa$  is also called Franck-Condon factor which describes the overlap of the phonon wavefunctions, and it directly influences the effective electronic coupling  $\tilde{J}$ . And the spectrum functions are chosen to be super-Ohmic as

$$J_{mn}(\omega) = \gamma_{mn} \frac{\omega^3}{\omega_c^2} e^{-\frac{\omega}{\omega_c}}, (m, n = 1, 2), \quad (6)$$

where  $\gamma_{11}$  ( $\gamma_{22}$ ) signifies the dimensionless exciton (ICTS)-phonon coupling strength and  $\gamma_{12}$  measures couplings of system and bath shared between the two states  $|1\rangle$  and  $|2\rangle$ . As  $|1\rangle$  and  $|2\rangle$  refer to the exciton state and the ICTS respectively, hereafter,  $\gamma_{11}$  and  $\gamma_{22}$  are both named system-bath coupling strength for brevity. Note that the interaction Hamiltonian is

dominated by site energy fluctuations and  $|1\rangle$  and  $|2\rangle$  interact with a common bath, therefore the energy fluctuations on the two states can have cross correlations. Consequently, the dimensionless  $\gamma_{12}$  is utilized to characterize the correlated fluctuations, whose amplitude is always smaller than that of the total fluctuations on each state, i.e.,  $\gamma_{12} \leq \sqrt{\gamma_{11}\gamma_{22}}$ . Thus we define a cross-correlation coefficient to describe bath correlation effects:

$$c = \frac{\gamma_{12}}{\sqrt{\gamma_{11}\gamma_{22}}}. \quad (7)$$

$c = -1, 0, 1$  corresponds to fully anti-correlated bath, independent(uncorrelated) bath and fully correlated bath, respectively. For numerical simulations, we assume that the two states interact with the phonon bath via the same spectral density, i.e.,  $\gamma_{11} = \gamma_{22} = \gamma$ . In this condition, the dynamics of a single excitation is fully decoupled from the bath for the case of  $\gamma = 0$  or fully correlated bath.

### C. Polaron master equation

After the polaron transformation  $\tilde{H} = e^S H e^{-S}$ , the renormalized  $\tilde{H}_{sb}$  can be taken as a perturbation term since the thermal average  $\langle \tilde{H}_{sb} \rangle = 0$ . With the Born-Markov approximation, the polaron master equation for charge transfer process between  $|1\rangle$  and  $|2\rangle$  can be obtained

$$\begin{aligned} \frac{d\rho'_s(t)}{dt} = & -i [\tilde{H}_s, \rho'_s(t)] - \sum_{i,j=z,\pm} [\Gamma_{ij}^+ \tau_i \tau_j \rho'_s(t) \\ & + \Gamma_{ji}^- \rho'_s(t) \tau_j \tau_i - \Gamma_{ji}^- \tau_i \rho'_s(t) \tau_j - \Gamma_{ij}^+ \tau_j \rho'_s(t) \tau_i], \end{aligned} \quad (8)$$

where  $\Gamma_{ij}^\pm$  are time-dependent rates related to bath correlation function. We define  $\rho'_s(t)$  as the reduced system density matrix in the polaron frame and define a new set of Pauli operators as

$$\begin{aligned} \tau_+ &= |+\rangle \langle -|, \\ \tau_- &= |- \rangle \langle +|, \\ \tau_z &= |+\rangle \langle +| - |- \rangle \langle -|, \end{aligned} \quad (9)$$

where we have moved into the renormalized exciton basis in which  $\tilde{H}_s |\pm\rangle = \varepsilon_\pm |\pm\rangle$ . In appendix A, we show the detailed derivations of Eq. (8).

In this paper, we are interested in how the phonon modes of LTB3 affects the charge transfer process of exciton-ICTS system. For the other three baths coupled with the system: HTB, LTB1 and LTB2, the Hamiltonians are respectively given by

$$\begin{aligned} H_h &= \sum_k \omega_{hk} a_{hk}^\dagger a_{hk} + (g_{hk} a_{hk}^\dagger |0\rangle \langle 1| + g_{hk}^* |1\rangle \langle 0| a_{hk}), \\ H_{c1} &= \sum_k \omega_{c1k} a_{c1k}^\dagger a_{c1k} + (g_{c1k} a_{c1k}^\dagger |\alpha\rangle \langle 2| + g_{c1k}^* |2\rangle \langle \alpha| a_{c1k}), \\ H_{c2} &= \sum_k \omega_{c2k} a_{c2k}^\dagger a_{c2k} + (g_{c2k} a_{c2k}^\dagger |0\rangle \langle \beta| + g_{c2k}^* |\beta\rangle \langle 0| a_{c2k}), \end{aligned} \quad (10)$$

where  $a_{hk}^\dagger$  ( $i = h, c1, c2$ ) is the creation operator of  $i$ th bath mode with the eigenfrequency  $\omega_{ik}$  and  $g_{ik}$  the corresponding coupling constant with the system. We adopt the local Liouville operator to phenomenologically describe the corresponding dissipative transition processes [69, 70]:

$$\begin{aligned} L_i(\rho) = & \frac{\gamma_i}{2} [(n_i + 1)(2O_i^- \rho O_i^+ - \{O_i^+ O_i^-, \rho\}) \\ & + n_i(2O_i^+ \rho O_i^- - \{O_i^- O_i^+, \rho\})], \end{aligned} \quad (11)$$

where  $i = h, c1, c2$  corresponds to the high temperature photon bath, the first and second low temperature phonon bath, respectively,  $\gamma_i$  and  $n_i$  are the corresponding dissipative rate and average photon(phonon) number. The system operators are defined as  $O_h^+ = |1\rangle \langle 0|$ ,  $O_{c1}^+ = |2\rangle \langle \alpha|$  and  $O_{c2}^+ = |\beta\rangle \langle 0|$  respectively.

Superoperator  $L_\Gamma$  describes the process that the electron is released from the system to drive a chain of sequence chemical reactions, i.e., to perform work:

$$L_\Gamma(\rho) = \frac{\Gamma}{2} [|\beta\rangle \langle \alpha| \rho |\alpha\rangle \langle \beta| - \rho |\alpha\rangle \langle \alpha| - |\alpha\rangle \langle \alpha| \rho], \quad (12)$$

It leads to the electronic current proportional to the relaxation rates  $\Gamma$ .

### D. Definitions of effective voltage and power

TABLE I: Parameters used in the numerical simulations.

Parameters	Units	Values
$E_{10}$	$\text{cm}^{-1}$	14,856
$E_{1\alpha}$	$\text{cm}^{-1}$	1,611
$E_{\beta 0}$	$\text{cm}^{-1}$	1,611
$E_{12}$	$\text{cm}^{-1}$	120
$J$	$\text{cm}^{-1}$	30
$\omega_c$	$\text{cm}^{-1}$	100
$\gamma_h$	$\text{cm}^{-1}$	0.005
$\gamma_{c1}$	$\text{cm}^{-1}$	140
$\gamma_{c2}$	$\text{cm}^{-1}$	200
$n_h$		60,000
$n_{c1}$		$7.8 \times 10^{-4}$
$n_{c2}$		$4.4 \times 10^{-4}$

In the reaction center, secondary charge separation and the following electron's being released to perform work induce a current which can be thought to flow cross a load connecting  $|\alpha\rangle$  and  $|\beta\rangle$ . Introducing an effective voltage  $V$  as a drop of the electrostatic potential across the load, we yield

$$eV = E_\alpha - E_\beta + k_B T \ln \frac{\rho_{\alpha\alpha}}{\rho_{\beta\beta}} \quad (13)$$

for our model, where  $e$  is the electric charge,  $E_i$  is the energy of state  $|i\rangle$  and  $\rho_{ii}$  is the population of state  $|i\rangle$  ( $i = \alpha, \beta$ ). With the current (Eq. (1)) and voltage, the power output can be calculated as

$$P = j \cdot V. \quad (14)$$

The performance of our QHE can be assessed in terms of the photovoltaic properties of PSII RC complex, i.e., the steady-state current-voltage ( $j - V$ ) and power-voltage ( $P - V$ ) characteristics. Using the steady-state solution, we plot the  $j - V$  curve and power at increasing rate  $\Gamma$ , while keep the other parameters fixed:  $\Gamma \rightarrow 0$  ( $j \rightarrow 0$ ) corresponds to the open-circuit case, and in the short-circuit case,  $V \rightarrow 0$ .

The parameters used in numerical simulations are listed in Table I. These parameters are reported in recent literatures [35, 71–73] and they are used in the simulation in [35, 74–76]. The energy differences are defined as  $E_{ij} = E_i - E_j$ .

### III. RESULTS AND DISCUSSIONS

In the polaron theory, the unitary transformation effectively changes the basis to the polaron basis including the exciton/charge transfer states and their associated displaced phonon modes. The thermal-averaged renormalized electronic coupling incorporates temperature and system-bath coupling dependence into the zero-order transformed Hamiltonian to evaluate the effects of thermal fluctuations on the eigenstates and equilibrium structures of the exciton-ICTS dimer system. We can predict that the renormalized electronic coupling goes to 0 at large temperature and system-bath couplings. In this section, we investigate how the temperature and system-bath coupling strength affect the effective coupling  $\tilde{J}$  (or Franck-Condon factor  $\kappa$ ), coherence and dynamical localization of the exciton-ICTS dimer system, and therefore,  $j - V$  and  $P - V$  characteristics as well.

#### A. Effective electronic coupling, coherence and delocalization length

Fig. 3 exhibits the effects of temperature  $T$  and system-bath coupling strength  $\gamma$  on Franck-Condon factor  $\kappa$ . We see that  $\kappa$  diminish to 0 when either  $T$  or  $\gamma$  increases. From Eq. (5), we can also conclude that  $\kappa$  decays to 0 at high temperature or strong system-bath coupling. This leads to decreasing effective electronic coupling  $\tilde{J}$  at either of these two limits and therefore, influences the performance of QHE which will be discussed in details in the following section. The equilibrium

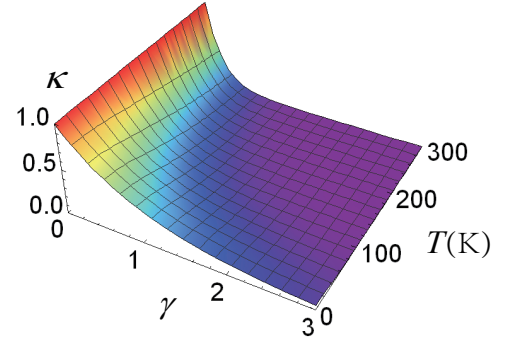


FIG. 3: (Color online) Franck-Condon factor  $\kappa$  as a function of temperature  $T$  and system-bath coupling  $\gamma$  with cross-correlation coefficient  $c = 0$ .

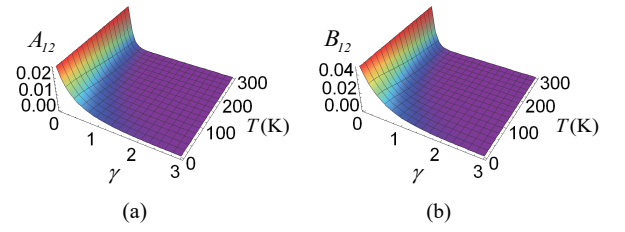


FIG. 4: (Color online) Coherence of the exciton-ICTS dimer system as a function of temperature  $T$  and system-bath coupling  $\gamma$ . (a) Real part of off-diagonal density matrix element:  $A_{12} = \text{Re}[\rho_{12}]$ . (b) Imaginary part of off-diagonal density matrix element:  $B_{12} = \text{Im}[\rho_{12}]$ . The cross-correlation coefficient  $c = 0$ .

structure of the exciton-ICTS dimer system are also affected by the temperature and system-bath coupling strength dependence of the effective coupling  $\tilde{J}$  (or  $\kappa$ ) as shown in Fig. 4. The coherence elements  $A_{12}$  and  $B_{12}$  of the equilibrium density matrix are illustrated in Fig. 4 (a) and (b) respectively, from which we conclude that the coherence decays to zero with increasing temperature or system-bath coupling strength. Therefore, strong system-bath coupling deteriorates the coherence of the exciton-ICTS dimer system. This is owing to dynamical energy fluctuations induced by the phonon bath. To explore the role of temperature and system-bath coupling strength in the system equilibrium structure, we also adopt the concept of delocalization length  $L$ , defined as the inverse participation of the eigenstate ( $|+\rangle$  or  $|-\rangle$  in our model):

$$L = \frac{1}{|\langle 1 | \pm \rangle|^4 + |\langle 2 | \pm \rangle|^4}. \quad (15)$$

In the renormalized exciton basis,  $\tilde{H}_s |\pm\rangle = \varepsilon_\pm |\pm\rangle$  with

$$\begin{aligned} |+\rangle &= \cos \frac{\theta}{2} |1\rangle + \sin \frac{\theta}{2} |2\rangle, \\ |-\rangle &= \sin \frac{\theta}{2} |1\rangle - \cos \frac{\theta}{2} |2\rangle, \end{aligned} \quad (16)$$

(see appendix A Eq. (A3)). Consequently, delocalization length  $L$  is given by

$$L = \frac{1}{\left|\cos \frac{\theta}{2}\right|^4 + \left|\sin \frac{\theta}{2}\right|^4} \quad (17)$$

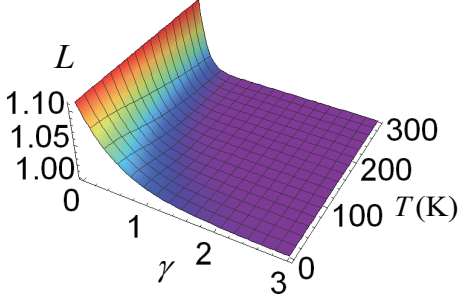


FIG. 5: (Color online) Delocalization length of the exciton-ICTS dimer system as a function of temperature  $T$  and system-bath coupling  $\gamma$ . The cross-correlation coefficient  $c = 0$ .

In Fig. 5, we plot the delocalization length as a function of temperature  $T$  and system-bath coupling strength  $\gamma$ . It is observed that, as  $T$  or  $\gamma$  increases, the delocalization length decreases to 1, which means eigenstates are completely localized on  $|1\rangle$  and  $|2\rangle$ . This also can be attributed to the bath-induced energy fluctuations. We see that in the polaron theory, this localization effect manifested by the renormalization of the effective electronic coupling  $\tilde{J}$  is embodied in the zero-order transformed Hamiltonian which is an advantage of this approach. In the following discussion, we apply dynamical localization to characterize the impact of phonon bath, giving explanations of various dynamical behaviors.

### B. Steady-state $j$ - $V$ and $P$ - $V$ characteristics

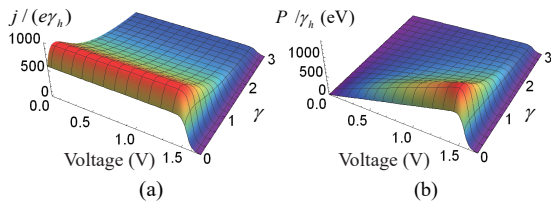


FIG. 6: (Color online) Steady-state  $j$ - $V$  (a) and  $P$ - $V$  (b) characteristics of QHE as a function of system-bath coupling strength  $\gamma$  with cross-correlation coefficient  $c = 0$  and temperature  $T = 300$  K.

Fig. 6 (a) and (b) show steady-state  $j$ - $V$  and  $P$ - $V$  characteristics respectively, as a function of system-bath coupling strength  $\gamma$ . At weak system-bath couplings, the current and power increases with  $\gamma$ . This can be explained from the point of view of noise-assisted transport extensively reported in the previous works [20, 21, 23, 77, 78]. The range of on-site energies of the two states are broadened due to bath-induced energy fluctuations, which leads to the overlap of  $|1\rangle$  and  $|2\rangle$

in energy and thus increases transfer rate between the two states enhancing steady-state  $j$ - $V$  and  $P$ - $V$  characteristics of QHE. If  $\gamma$  continues to increase, the effect of resonant mode decreases as the energy of each state is distributed over a very large interval. And meanwhile, increasing system-bath coupling strength  $\gamma$  also deteriorates the coherence of the exciton-ICTS dimer system due to bath-induced fluctuations, or equivalently, leads to dynamical localization that the electronic eigenstates are localized on the state  $|1\rangle$  or  $|2\rangle$  which impedes charge transfer process and thus lessens the current and power generated. Thus, there exists an optimal value of  $\kappa$  at which noise-assisted effect and dynamical localization reach a balance producing the maximal current and power. Interestingly, these two effects both originate from the fluctuations induced by phonon bath. The fluctuations can promote or impede the current and power according to the values of  $\gamma$ .

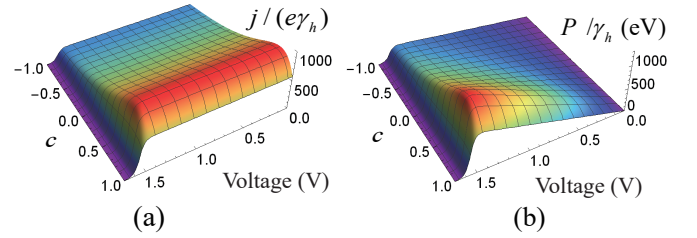


FIG. 7: (Color online) Steady-state  $j$ - $V$  (a) and  $P$ - $V$  (b) characteristics of QHE as a function of bath cross-correlation coefficient  $c$  (defined as Eq. (7)) with system-bath coupling strength  $\gamma = 1$  and temperature  $T = 300$  K.

In Fig. 6, we set the cross-correlation coefficient  $c = 0$ , i.e., the bath is uncorrelated. Recent experiments have revealed that, besides electronic coherence, highly correlated fluctuations of the bath should also be included to explain the observed long-lasting excitonic coherence. Motivated by these findings, the effect of bath correlations on the dynamics of EET in photosynthetic light-harvesting complexes has attracted great interest recently [55, 63, 78–83]. Next we shed light on the effects of bath correlation.

In Fig. 7, we plot steady-state  $j$ - $V$  (a) and  $P$ - $V$  (b) characteristics as a function of cross-correlation coefficient  $c$ . Similar to the case of  $\gamma$ , the current or power is not a monotonic function of  $c$ . We comprehend this by carefully examining Eq. (5), which can be analytically calculated as

$$\kappa = \exp \left[ -\frac{(\gamma_{11} - 2c\sqrt{\gamma_{11}\gamma_{22}} + \gamma_{22})}{2} \left( -1 + \frac{\psi' \left( \frac{1}{\beta\omega_c} \right)}{(\beta\omega_c)^2} \right) \right]. \quad (18)$$

where  $\psi'$  denotes the trigamma function [84]. We set  $y = \gamma_{11} - 2c\sqrt{\gamma_{11}\gamma_{22}} + \gamma_{22}$ . Since the assumption  $\gamma_{11} = \gamma_{22} = \gamma$  has been made, we have  $y = 2\gamma(1 - c)$ . From Fig. 7, the maximal current and power appears when  $c \sim 0.8$  and this gives  $y \sim 0.4$  with the fixed system-bath coupling  $\gamma = 1$  when temperature  $T = 300$  K. And from Fig. 6, taking  $\gamma \sim 0.2$  yields the maximal current and power and thus  $y \sim 0.4$  with



the fixed cross-correlation coefficient  $c = 0$  when temperature  $T = 300$  K, in accordance with the results of Fig. 7. Thus  $y$  can be regarded as a whole which we name as effective system-bath coupling factor. It characterizes how the exciton-ICTS dimer system interacts with bath modes, including the effects of both individual exciton- or ICTS-phonon coupling (denoted by  $\gamma_{11}$  and  $\gamma_{22}$  respectively) and correlated fluctuations of bath modes (denoted by  $\gamma_{12}$  or  $c$ ) on system-bath interaction. For a certain temperature, there exists an optimal value for  $y$ . For Fig. 6 and Fig. 7 with fixed temperature  $T = 300$  K, we have evaluated the optimal value of the effective system-bath coupling strength  $y$  to be 0.4.  $y \sim 0 - 0.4$  is noise-assisted regime in which the current and power increases with  $y$ . At  $y = 0.4$ , noise-assisted effects and dynamical localization reach a good balance generating maximal current and power. When  $y > 0.4$ , dynamical delocalization dominates the charge transfer process, increasing  $y$  giving rise to enhanced fluctuations which hinders the QHE performance. Therefore, we conclude from  $y = 2\gamma(1 - c)$  that the effect of bath correlation  $c$  on current and power is incorporated in the effective system-bath coupling strength  $y$ .  $c$  effectively strengthens or weakens  $\gamma$  giving different values of  $y$  and thus impacts  $j - V$  and  $P - V$  characteristics. Now, we analyse Fig. 6 in terms of effective system-bath coupling factor  $y$ : when  $T = 300$  K, for fixed  $c = 0$ ,  $\gamma \sim 0 - 0.2$  is the noise-assisted transport regime ( $y \sim 0 - 0.4$ ). If  $\gamma$  increases further,  $y$  locates in the dynamical localization regime where larger  $\gamma$  reduces the current and power. Similarly, Fig. 7 can be reinterpreted as follows: when  $c = 1$ , we obtain  $y = 0$  which corresponds to  $\gamma = 0$  in Fig. 6. As  $c$  gradually decreases,  $y$  first increases to its optimal value corresponding to the noise-assisted transport regime, and then increases into the dynamical localization regime. Thus as  $c$  decreases, the current and power increases first and then decreases. Based on these discussions, we further inspect how  $\gamma$  and cross-correlation coefficient  $c$  conspire to affect the CT process in Sec. III C.

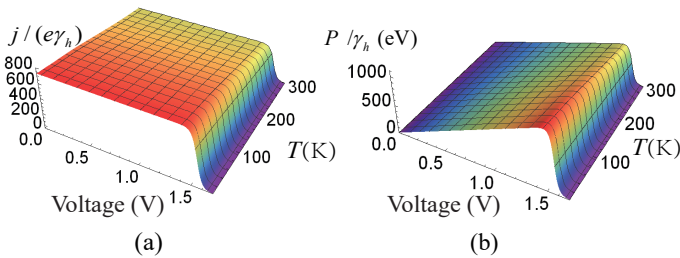


FIG. 8: (Color online) Steady-state  $j - V$  (a) and  $P - V$  (b) characteristics of QHE as a function of temperature  $T$  with the system-bath coupling strength  $\gamma = 1$  and cross-correlation coefficient  $c = 0$ .

In Fig. 8, we plot steady-state  $j - V$  and  $P - V$  characteristics for varying temperature  $T$ . We have learned from above discussion that for the fixed temperature  $T = 300$  K, the optimal  $y$  takes 0.4. The dynamics of the exciton-ICT dimer system includes noise-assisted and dynamical localization regime. From Fig. 8, however, we see that as temperature increases, the current and power decrease monotonically. We

can explain as follows: higher temperature reduces effective electronic coupling  $\tilde{J}$  from Fig. 3 or Eq. (18), which in turn deteriorates coherence or leads to dynamical localization due to enhanced bath-induced fluctuations. But this raises a question that: since both higher temperature and larger  $\gamma$  (or  $y$ ) lead to dynamical localization, does the dynamics of exciton-ICT dimer system converts between noise-assisted and dynamical localization regime with varying  $T$  just as that with  $\gamma$  (or  $y$ )? Or how can the effect of temperature be reflected? Based on this question, we investigate how  $\gamma$ ,  $c$  and  $T$  conspire to affect the QHE performance in Sec. III D.

### C. Combined effects of $\gamma$ , $c$

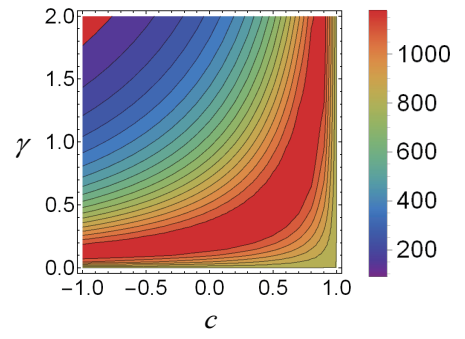


FIG. 9: (Color online) The power generated by QHE as a function of cross-correlation coefficient  $c$  and system-bath coupling strength  $\gamma$ .

In Fig. 9, we plot the power of our QHE model as a function of system-bath coupling strength and bath correlations, from weak ( $\gamma \sim 0$ ) to strong ( $\gamma = 2$ ) coupling, and from fully correlated bath ( $c = 1$ ) to fully anti-correlated bath ( $c = -1$ ). Although, we can also plot the current, basically the variation of current is the same as that of power. Thus we only focus on the behaviors of the power generated.

The QHE performance shows strong dependence on both  $\gamma$  and  $c$  and various dynamical regimes which can be interpreted in terms of what we have learned from Eq. (18) in Section III B. Nevertheless, for weak and strong coupling strength, the dependence of the current and power on bath correlation is remarkably different.

From Fig. 9, when  $\gamma$  is very small ( $< 0.1$ ), i.e., at weak system-bath couplings, the power generated by the QHE model monotonically decreases with increasing  $c$ . That's to say, the power reaches maximum when the bath is fully anti-correlated. We see that when  $\gamma$  is very small, the effective system-bath coupling  $y$  locates in noise-assisted transfer regime ( $y \sim 0 - 0.4$ ), increasing  $y$  leads to higher performance of QHE. And according to Eq. (18) or the effective system-bath coupling expression  $y = 2\gamma(1 - c)$ ,  $y$  is a monotonically decreasing function of  $c$ , thus increasing  $c$  gives smaller effective system-bath coupling factor  $y$ , leading to reduced power. Also, we can learn from Sec. III B that, anti-correlated bath gives rise to enhanced fluctuations in the effective coupling



$\tilde{J}$  while correlated bath suppress fluctuations. As the optimal effective system-bath coupling factor takes  $y \sim 0.4$  when  $T = 300$  K, it is straightforward to evaluate the optimal value of  $c$  as smaller than  $-1$ , consequently the anti-correlated bath with enhanced fluctuations in the effective electronic coupling  $\tilde{J}$  maximizes the QHE performance. And when  $c$  increases from  $-1$  to  $1$ , the power monotonically decreases.

However, when  $\gamma$  gets larger, for example,  $\gamma = 1$ , the power first increases to a maximum and then decreases with increasing  $c$  from Fig. 9. According to the expression  $y = 2\gamma(1 - c)$ , with  $\gamma = 1$ ,  $c \sim 0.8$  obtains the optimal effective system-bath coupling factor  $y$ , in agreement with what can be observed from Fig. 9.  $c \sim -1 - 0.8$  corresponds to dynamical localization regime in which anti-correlated bath with enhanced fluctuations will certainly reduce the power, while  $c \sim 0.8 - 1$  noise-assisted regime, i.e. varying  $c$  between  $-1$  and  $1$  obtain a range of  $y$  that contains the optimal value  $y = 0.4$ . As a consequence, when  $\gamma = 1$ , the power is not a monotonic function of  $c$ , just as observed in Fig. 9. The bath-induced fluctuations promote or impede the QHE model for different values of  $c$ .

Next, we discuss the case when  $c$  is fixed observed in Fig. 9. Similarly, when the bath is basically correlated ( $c \sim 1$ ), the power monotonically increases with  $\gamma$  since when  $c \sim 1$ ,  $y$  is in the range of noise-assisted transport regime unless  $\gamma$  becomes extremely large. Increasing  $y$  produces larger power. And  $y = 2\gamma(1 - c)$  is a monotonically increasing function of  $\gamma$ . Therefore, increasing  $\gamma$  leads to enhanced fluctuations promoting the QHE performance. Otherwise ( $c < 0.85$ ), when  $c = 0.5$  for example, the power first increases to the maximum and then decreases with increasing  $\gamma$ . As  $c = 0.5$  gives  $y = \gamma$ , with increasing  $\gamma$ ,  $y$  increases from noise-assisted transport regime to dynamical localization regime, passing the optimal value  $y = 0.4$ . Therefore, when  $c < 0.85$ , the power is not a monotonic function of  $\gamma$ .

What we have discussed above is based on a fixed temperature  $T = 300$  K. It is clear from Eq. (18) that temperature also affects the thermal averaged Franck-Condon factor  $\kappa$ . So it is interesting to study how temperature works together with system-bath coupling  $\gamma$  and cross-correlation coefficient  $c$  to affect QHE behaviors.

#### D. Effects of temperature $T$

Fig. 10 is plotted for the power generated by QHE as a function of temperature  $T$  and system-bath coupling strength  $\gamma$  for the uncorrelated bath ( $c = 0$ ). At any temperature, the power increases first to a maximal value and then gradually decreases with  $\gamma$ , just as revealed by Fig. 6 and Fig. 9. In contrast, the power decreases with temperature monotonically when  $\gamma$  is not very large, i.e., the dynamics of exciton-ICTS dimer system locates in the dynamical localization regime in this case. However we can observe that, temperature affects the optimal value of  $\gamma$  that yields the maximal power. We revisit Eq. (18) to give an explanation. It is easy to know that an optimal effective system-bath coupling strength  $y$  correspondingly gives an optimal Franck-Condon factor  $\kappa$  for a certain temperature  $T$ . The effects of phonon bath LTR3 on the exciton-ICT dimer

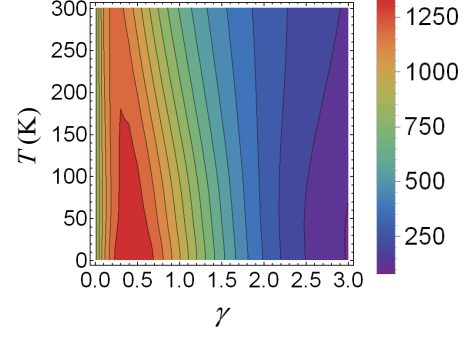


FIG. 10: (Color online) The power generated by QHE as a function of temperature  $T$  and system-bath coupling strength  $\gamma$  for the uncorrelated bath ( $c = 0$ ).

system are fully embodied in Franck-Condon factor  $\kappa$ . Since  $\tilde{J} = J\kappa$ ,  $\kappa$  directly influences the effective electronic coupling  $\tilde{J}$  which determines the extent of delocalization for the dimer system induced by fluctuations. We can estimate the optimal  $\kappa$  (denoted by  $\kappa_{opt}$ ) for different temperatures from Fig. 10 in which cross-correlation coefficient  $c$  are set to be zero. For  $T = 300$  K, the maximal power appears at  $\gamma \sim 0.25$ , this yields  $\kappa_{opt} \sim 0.34$ . Similarly, for  $T = 200$  K,  $\kappa_{opt} = 0.41$ , and for  $T = 50$  K,  $\kappa_{opt} = 0.57$ . In physics, this indicates that temperature influences the balance between noise-assisted transport effects and dynamical localization, though the dynamics can not convert between the two regimes with temperature just as that with system-bath coupling and bath-correlation.

As system-bath coupling further increases ( $\gamma > 2.2$ ), it is interesting to observe that the power gets slightly larger with increasing temperature. Actually, we ignore another effect induced by temperature in the discussions above. That is: higher temperature gives rise to larger effective transfer rates concerned with LTR1 and LTR2, which enhances QHE performance at both weak and strong system-bath coupling regimes. We have learned from Eq. (18) that, Franck-Condon factor  $\kappa$  is a monotonic decreasing function of temperature indicating that higher temperature leads to strong dynamical localization. The promotion and impediment roles that temperature plays in energy transfer process depends on the extent of dynamical localization of the exciton-ICT dimer system. So Fig. 10 can be explained as follows: at weak system-bath couplings, the excitons are still partially dynamical delocalized, thus higher temperatures will lead to stronger localization. Impediment effects of temperature surpass its promotion effects. When  $\gamma$  becomes large enough, the eigenstates have been fully localized. Further increasing temperature can not reduce the transfer rate of exciton-ICT dimer system, but promote transfer process influenced by LTR1 and LTR2. Therefore, as shown in Fig. 10, when  $\gamma > 2.2$ , the power gets larger with increasing temperature.

Fig. 11 illustrates the power generated by QHE as a function of temperature  $T$  and cross-correlation coefficient  $c$  with the system-bath coupling  $\gamma = 1$ . The power increases to maximal values and then gradually decrease with  $c$ , in accordance with the results of Fig. 7 and Fig. 9. Similarly, temperature

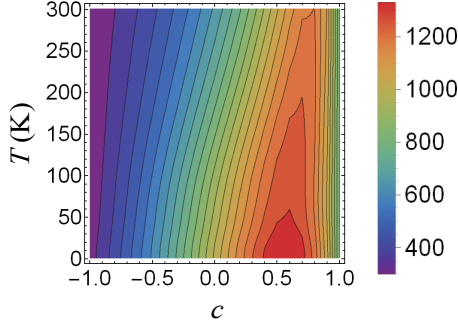


FIG. 11: (Color online) The power generated by QHE as a function of temperature  $T$  and cross-correlation coefficient  $c$  with the system-bath coupling strength  $\gamma = 1$ .

affects the optimal value of  $c$  that yields the maximal power which also can be explained as the effect of temperature on the balance between noise-assisted transport and dynamical localization. Meanwhile, the power monotonically decreases with temperature. This is because the eigenstates of the exciton-ICTS dimer system are still partially dynamical delocalized for the given range of parameters ( $\gamma = 1$  and  $-1 \leq c \leq 1$ ), higher temperature only leads to enhanced fluctuations that gives rise to strong dynamical localization. Although increasing  $T$  promotes effective transfer rates concerned with LTR1 and LTR2, it is not as remarkable as the impediment effects induced by strong dynamical localization.

### E. Effective voltage $V$

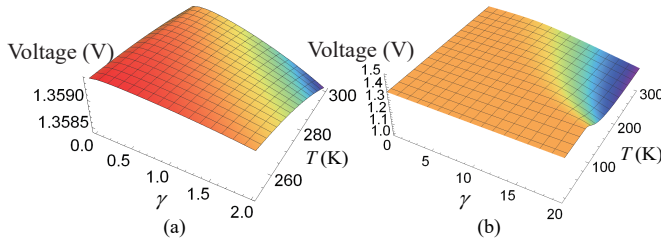


FIG. 12: (Color online) The effective voltage of QHE as a function of temperature  $T$  and system-bath coupling strength  $\gamma$  for the uncorrelated bath ( $c = 0$ ) with different parameter ranges for (a) and (b).

Having investigated the power as a function of system-bath coupling  $\gamma$ , cross-correlation coefficient  $c$  and temperature  $T$ , another question arises: how is the effective voltage  $V$  influenced by these parameters? Since  $c$  has been incorporated in the effective system-bath coupling  $\gamma$ , effectively strengthening or weakening  $\gamma$ , we only focus on the impact of temperature and system-bath coupling on the voltage  $V$ . The results are illustrated in Fig. 12. At high temperature ( $T = 300$  K for example in Fig. 12 (a)), the voltage increases very slightly to a maximum at first, and then decreases gradually just as the behaviors of the power with  $\gamma$  and the physics is the same. But

the changing rate is much slower when  $\gamma$  is not very large. The effective voltage of our QHE model exhibits superior robustness with respect to the bath conditions. Thus in Fig. 9- Fig. 11, we only plot the power as a function of different parameters. Nevertheless, with  $\gamma$  increasing further ( $\gamma > 5$ ), the voltage decreases almost linearly with  $\gamma$  (Fig. 12 (b)) indicating the population on the secondary charge separation state  $|\alpha\rangle$  decreases exponentially. In this case, energy transfer of the exciton-ICTS dimer state is completely suppressed by the extremely large fluctuations induced by phonon bath leading to sharply reduced population on the secondary charge separation state  $|\alpha\rangle$  and in turn  $\rho_{\alpha\alpha}$  decreases to zero quickly. The current or power also diminishes to zero. Therefore, the population on  $|\beta\rangle$  is hardly influenced by that on  $|\alpha\rangle$  but determined by the transition process subjected to LTB2 denoted by the Liouville operator  $L_{c2}$ .  $L_{c2}$  guarantees a certain value of population on  $|\beta\rangle$ , meanwhile  $\rho_{\alpha\alpha}$  decays to zero when  $\gamma$  gets extremely large. Therefore, according to the definition  $eV = E_{\alpha} - E_{\beta} + k_B T \ln \frac{\rho_{\alpha\alpha}}{\rho_{\beta\beta}}$ , it is easy to understand the variation of voltage with  $\gamma$ . Return to the case when  $\gamma$  is not very large. From Fig. 6-Fig. 8, the current  $j$  (or the population  $\rho_{\alpha\alpha}$ ) remains large when  $\gamma < 3$ . It is  $\rho_{\alpha\alpha}$  that mainly influences the population on  $|\beta\rangle$  by the relaxation process  $|\alpha\rangle \rightarrow |\beta\rangle$ , rather than the transition process induced by LTB2. Thus, the ratio  $\frac{\rho_{\alpha\alpha}}{\rho_{\beta\beta}}$  will not change significantly under this circumstances. In other words,  $V$  is robust against the bath noise as long as  $\gamma$  is not too large. At low temperature, the tendencies are generally the same except that the voltage begins to decrease quickly at larger  $\gamma$ . This is because at large system-bath coupling,  $\rho_{\alpha\alpha}$  is already very small and has a negligible impact on  $\rho_{\beta\beta}$ , but lower temperature leads to smaller population on  $|\beta\rangle$  than high temperature. As a consequence,  $\rho_{\alpha\alpha}$  should decrease to a smaller value which requires larger  $\gamma$ . We see that the physics underlying these results on the effective voltage  $V$  also lies in the dynamical location due to bath-induced fluctuations.

## IV. CONCLUSION

In this paper, we apply polaron master equation to analyse the effects of system-bath couplings on charge transfer processes in PS II RC for a wide parameter range. Effects of bath correlations and temperature of phonon bath are also included.

Our analysis shows that temperature and system-bath coupling determine the effective electronic coupling thus influencing the equilibrium structure and dynamical localization, and in turn leading to various behaviors of QHE performance. The results reveal that system-bath coupling can promote or impede the performance of QHE depending on the coupling strength. It is a result of a balance of noise-assisted transport and dynamical localization. The effects of bath correlation, denoted by cross-correlation coefficient  $c$ , is incorporated in the effective system-bath coupling  $\gamma$ . Similarly, the power generated increases or decreases with  $c$  depending on the different system-bath coupling strength regimes. Temperature affects the optimal value of  $\gamma$  that yields the maximal current and power. In other words, temperature changes the balance of noise-assisted transport and dynamical localization

effects. In addition, higher temperature also enhance transfer process related to LTR1 and LTR2. Whether it can promote or impede the performance of QHE depends on the extent of localization. The effective voltage  $V$  changes very slowly when system-bath coupling strength is not very large, i.e.,  $V$  of our QHE model is robust against the bath noise. With further increasing  $\gamma$ ,  $V$  decreases quickly which should be explained by considering the impact of dissipative phonon bath LTB2.

In summary, system-bath coupling  $\gamma$ , cross-correlation coefficient  $c$  and temperature  $T$  conspire to affect the charge transfer process, thus showing various dynamical regimes from which two important mechanisms dominating the transfer process in photosynthetic complexes can be extracted. The first one is resonance energy transfer mechanism. In our model, for example, resonance energy transfer requires the same energy of  $|1\rangle$  and  $|2\rangle$ . This mechanism is manifested by the noise-assisted transfer effect since the range of on-site energies of the two states are broadened due to bath-induced energy fluctuations which leads to the overlap of  $|1\rangle$  and  $|2\rangle$  in energy. The second one is the dynamical localization which incorporates the effects system-bath coupling, bath correlation and temperature. For different values of  $\gamma$ ,  $c$ , these two mechanisms interpret various dynamical regimes, and  $T$  modulates the relative strength of the two mechanism. Furthermore, we attribute the two mechanisms to one physical origin: bath-induced fluctuations. Dynamical energy fluctuations, on the one hand, gives rise to broadened on-site energies bringing about noise-induced transport effect. On the other hand, fluctuations reduce the effective electronic coupling  $\tilde{J}$  leading to dynamical localization.

We hope that our work give helpful insights into the charge transfer mechanisms in photosynthetic reaction centers and will be constructive for designing novel nanofabricated structures for quantum transport and optimized solar cells.

## V. ACKNOWLEDGMENTS

This work is supported by National Natural Science Foundation of China (NSFC) under Grants No. 11175032, and No. 61475033.

### Appendix A: The derivation of Eq. (8)

Within the polaron frame, the thermal average of  $\tilde{H}_{sb}$  equals to 0, therefore the second-order perturbation theory can be applied.

To simplify further analysis, it is convenient to move into the renormalized exciton basis in which  $\tilde{H}_s|\pm\rangle = \varepsilon_\pm|\pm\rangle$  and transform into the interaction picture. With the Born-Markov approximation, the master equation for EET between  $|1\rangle$  and  $|2\rangle$  in the interaction picture is given by

$$\frac{d\rho'^I_s(t)}{dt} = - \int_0^\infty ds \text{Tr}\{[\tilde{H}_{sb}(t), [\tilde{H}_{sb}(t-s), \rho'^I_s(t) \otimes \rho'_b]]\} \rho'^I_s(t) \quad (\text{A1})$$

where  $\tilde{H}_{sb}(t) = e^{i(\tilde{H}_s + \tilde{H}_b)t} \tilde{H}_{sb} e^{-i(\tilde{H}_s + \tilde{H}_b)t}$ . Substitute the interaction Hamiltonian  $\tilde{H}_{sb}(t)$  into Eq. (A1), and then transform

back into the Schrödinger picture and finally obtain Eq. (8):

$$\begin{aligned} \frac{d\rho'_s(t)}{dt} = & -i[\tilde{H}_s, \rho'_s(t)] - \sum_{i,j=z,\pm} [\Gamma_{ij}^+ \tau_i \tau_j \rho'_s(t) \\ & + \Gamma_{ji}^- \rho'_s(t) \tau_j \tau_i - \Gamma_{ji}^- \tau_i \rho'_s(t) \tau_j - \Gamma_{ij}^+ \tau_j \rho'_s(t) \tau_i]. \end{aligned} \quad (\text{A2})$$

Here, the Pauli operators  $\tau_i$  are defined by Eq. (9) in which

$$\begin{aligned} |+\rangle &= \cos \frac{\theta}{2} |1\rangle + \sin \frac{\theta}{2} |2\rangle, \\ |-\rangle &= \sin \frac{\theta}{2} |1\rangle - \cos \frac{\theta}{2} |2\rangle, \end{aligned} \quad (\text{A3})$$

with  $\tan \theta = \frac{2\kappa J}{\tilde{\varepsilon}}$  and  $\tilde{\varepsilon} = \tilde{\varepsilon}_1 - \tilde{\varepsilon}_2$ . The time-dependent rates  $\Gamma_{ij}^\pm$  can be calculated via the bath correlation functions

$$\begin{aligned} \Gamma_{ij}^+ &= \frac{J^2}{4} \int_0^\infty ds \langle \xi_i(0) \xi_j(-s) \rangle, \\ \Gamma_{ij}^- &= \frac{J^2}{4} \int_0^\infty ds \langle \xi_i(-s) \xi_j(0) \rangle, \end{aligned} \quad (\text{A4})$$

with

$$\begin{aligned} \xi_z(t) &= \sin \theta (\tilde{B}(t) + \tilde{B}^\dagger(t)), \\ \xi_+(t) &= \tilde{B}^\dagger(t)(1 - \cos \theta) e^{i\Delta \varepsilon t} - \tilde{B}(t)(1 + \cos \theta) e^{i\Delta \varepsilon t}, \\ \xi_-(t) &= \tilde{B}(t)(1 - \cos \theta) e^{-i\Delta \varepsilon t} - \tilde{B}^\dagger(t)(1 + \cos \theta) e^{-i\Delta \varepsilon t}, \end{aligned} \quad (\text{A5})$$

where

$$\Delta \varepsilon = \varepsilon_+ - \varepsilon_- = \sqrt{4J^2\kappa^2 + (\tilde{\varepsilon}_1 - \tilde{\varepsilon}_2)^2}, \quad (\text{A6})$$

and  $\tilde{B}(t) = B(t) - \kappa$  with

$$\begin{aligned} B(t) &= e^{i\tilde{H}_{sb}t} B e^{-i\tilde{H}_{sb}t} \\ &= \exp\left[\sum_k \left(\delta g_{vk,12} b_k^\dagger e^{i\omega_{vk}t} - \delta g_{vk,12}^* b_k e^{-i\omega_{vk}t}\right)\right] \omega_{vk} \end{aligned} \quad (\text{A7})$$

We need to transform Eq. (8) back to the local frame. Since  $\sigma_z$  commutes with the polaron transformation operator, the population term is easily to be obtained:

$$\begin{aligned} \rho_{11}(t) &= Tr_{s+b}(\rho_{\text{tot}}(t) |1\rangle\langle 1|) \\ &= Tr_{s+b} \left( e^{i\sigma_z B/2} \rho'_{\text{tot}}(t) e^{-i\sigma_z B/2} |1\rangle\langle 1| \right) \\ &= Tr_{s+b} \left( \rho'_{\text{tot}}(t) e^{-i\sigma_z B/2} |1\rangle\langle 1| e^{i\sigma_z B/2} \right) \\ &= Tr_s(\rho'_s(t) |1\rangle\langle 1|). \end{aligned} \quad (\text{A8})$$

where  $\rho'_{\text{tot}}(t) = e^{-i\sigma_z B/2} \rho_{\text{tot}}(t) e^{i\sigma_z B/2}$  is the polaron-transformed density matrix for the dimer system and LTB3 with  $\rho_{\text{tot}}(t)$  the total density matrix in the local frame and in the same way,

$$\rho_{22}(t) = Tr_{s+b}(\rho'_s(t) |2\rangle\langle 2|). \quad (\text{A9})$$

Nevertheless,  $\sigma_x$  ( $\sigma_y$ ) does not commute with the polaron transformation operator. Consequently, the exact coherence terms can not be obtained. We can use the Born approximation  $\rho'_{\text{tot}}(t) \approx \rho'_s(t) \otimes \rho'_b$  to solve this problem. The Born approximation has already been used in deriving Eq. (8, assuming that the coupling between the system and bath is weak. As in the polaron transformation theory, the system-bath interaction term is reduced and can be treated as a perturbation, it is reasonable to be approximately factorize the density matrix in the polaron frame. Therefore, we obtain the coherence term of the reduced system density matrix in the local frame as

$$\begin{aligned}
 \rho_{12}(t) &= \text{Tr}_{s+b}(\rho_{\text{tot}}(t) |2\rangle \langle 1|) \\
 &= \text{Tr}_{s+b} \left( e^{i\sigma_z B/2} \rho'_{\text{tot}}(t) e^{-i\sigma_z B/2} |2\rangle \langle 1| \right) \\
 &= \text{Tr}_{s+b} \left( \rho'_{\text{tot}}(t) e^{-i\sigma_z B/2} |2\rangle \langle 1| e^{i\sigma_z B/2} \right) \quad (\text{A10}) \\
 &\approx \text{Tr}_{s+b} \left( \rho'_s(t) \otimes \rho'_b e^{-iB} |2\rangle \langle 1| \right) \\
 &= \kappa \text{Tr}_s (\rho'_s(t) |2\rangle \langle 1|).
 \end{aligned}$$

- 
- [1] H. van Amerongen, L. Valkunas, and R. van Grondelle, *Photosynthetic Excitons* (World Scientific, Singapore, 2000).
- [2] R. E. Blankenship, *Molecular Mechanisms of Photosynthesis* (Blackwell Science Ltd, Oxford, UK, 2002).
- [3] R. E. Blankenship, D. M. Tiede, J. Barber, G. W. Brudvig, G. Fleming, M. Ghirardi, M. R. Gunner, W. Junge, D. M. Kramer, A. Melis, T. A. Moore, C. C. Moser, D. G. Nocera, A. J. Nozik, D. R. Ort, W. W. Parson, R. C. Prince, and R. T. Sayre, *Science* **332**, 805 (2011).
- [4] E. Wientjes, H. van Amerongen, and R. Croce, *J. Phys. Chem.* **117**, 11200-11208, (2013).
- [5] D. Hayes, G. Panitchayangkoon, K.A. Fransted, J. R. Caram, J. Wen, K. F. Freed, and G. S. Engel, *New J. Phys.* **12**, 065042 (2010).
- [6] G. D. Scholes, G. R. Fleming, A. Olaya-Castro, and R. van Grondelle, *Nat. Chem.* **3**, 763 (2011).
- [7] N. Lambert, Y.-N. Chen, Y.-C. Cheng, C.-M. Li, G.-Y. Chen, and F. Nori, *Nat. Phys.* **9**, 10 (2013).
- [8] Y. Omar, M. Mohseni, G. S. E. Engel, and M. B. Plenio, *Quantum Effects in Biology* (Cambridge University Press, 2014).
- [9] T. Brixner, J. Stenger, H. M. Vaswani, M. Cho, R. E. Blankenship, and G. R. Fleming, *Nature* **434**, 625 (2005).
- [10] G. S. Engel, T.R. Calhoun, E. L. Read, T.-K. Ahn, T. Mančal, Y.-C. Cheng, R. E. Blankenship, and G. R. Fleming, *Nature (London)* **446**, 782 (2007).
- [11] T. R. Calhoun, N. S. Ginsberg, G. S. Schlau-Cohen, Y.-C. Cheng, M. Ballottari, R. Bassi, and G. R. Fleming, *J. Phys. Chem. B* **113**, 16291 (2009).
- [12] E. Collini, C. Y. Wong, K. E. Wilk, P. M. G. Curmi, P. Brumer, and G. D. Scholes, *Nature (London)* **463**, 644 (2010).
- [13] G. Panitchayangkoon, D. Hayes, K.A. Fransted, J. R. Caram, E. Harel, J. Wen, R. E. Blankenship, and G. S. Engel, *Proc. Natl. Acad. Sci. U.S.A.* **107**, 12766 (2010).
- [14] E. Harel and G. S. Engel, *Proc. Natl. Acad. Sci. U.S.A.* **109**, 706 (2012).
- [15] E. Romero, R. Augulis, V. I. Novoderezhkin, M. Ferretti, J. Thieme, D. Zigmantas, and R. van Grondelle, *Nat. Phys.* **10**, 676 (2014).
- [16] F. D. Fuller, J. Pan, A. Gelzinis, V. Butkus, S. S. Senlik, D. E. Wilcox, C. F. Yocum, L. Valkunas, D. Abramavicius, and J. P. Ogilvie, *Nat. Chem.* **6**, 706 (2014).
- [17] A. Olaya-Castro, C. F. Lee, F. F. Olsen, and N. F. Johnson, *Phys. Rev. B* **78**, 085115 (2008).
- [18] M. B. Plenio and S. F. Huelga, *New J. Phys.* **10**, 113019 (2008).
- [19] M. Mohseni, P. Rebentrost, S. Lloyd, and A. Aspuru-Guzik, *J. Chem. Phys.* **129**, 174106 (2008).
- [20] P. Rebentrost, M. Mohseni, I. Kassal, S. Lloyd, and A. Aspuru-Guzik, *New J. Phys.* **11**, 033003 (2009).
- [21] F. Caruso, A. W. Chin, A. Datta, S. F. Huelga, and M. B. Plenio, *J. Chem. Phys.* **131**, 105106 (2009).
- [22] A. Ishizaki and G. R. Fleming, *Proc. Natl. Acad. Sci. USA* **106**, 17255 (2009).
- [23] A. W. Chin, A. Datta, F. Caruso, S. F. Huelga, and M. B. Plenio, *New J. Phys.* **12**, 065002 (2010).
- [24] G. D. Scholes, *J. Phys. Chem. Lett.* **1**, 2 (2010).
- [25] S. Lloyd and M. Mohseni, *New J. Phys.* **12**, 075020 (2010).
- [26] J. Strumpfer, M. Sener, and K. Schulten, *J. Phys. Chem. Lett.* **3**, 536 (2012).
- [27] H. Dong, D.-Z. Xu, J.-F. Huang, and C.-P. Sun, *Light: Sci. Appl.* **1**, e2 (2012).
- [28] M. del Rey, A. W. Chin, S. F. Huelga, and M. B. Plenio, *J. Phys. Chem. Lett.* **4**, 903 (2013).
- [29] A. W. Chin, J. Prior, R. Rosenbach, F. Caycedo-Soler, S. F. Huelga, and M. B. Plenio, *Nat. Phys.* **9**, 113 (2013).
- [30] S. F. Huelga and M. B. Plenio, *Contemp. Phys.* **54**, 181 (2013).
- [31] M. O. Scully, *Phys. Rev. Lett.* **104**, 207701 (2010).
- [32] M. O. Scully, K. R. Chapin, K. E. Dorfman, M. B. Kim, and A. Svidzinsky, *Proc. Natl. Acad. Sci. U. S. A.* **108**, 15097 (2011).
- [33] Y. Zhang, S. Oh, F. H. Alharbi, G. Engel, and S. Kais, *Phys. Chem. Chem. Phys.* **17**, 5743C5750 (2015).
- [34] S. Ajisaka, B. Zunkovic, and Y. Dubi, *Sci. Rep.* **5**, 8312 (2015).
- [35] K. E. Dorfman, D. V. Voronine, S. Mukamel, and M. O. Scully, *Proc. Natl. Acad. Sci. U.S.A.* **110**, 2746 (2013).
- [36] R. Stones, H. Hossein-Nejad, R. van Grondelle, and A. Olaya-Castro, arXiv:1601.05260.
- [37] T. Renger and E. Schlodder, *J. Photochem. Photobio. B* **104**, 126, (2011).
- [38] V. I. Novoderezhkin, E. G. Andrizhiyevskaya, J. P. Dekker, and R. van Grondelle, *Biophys. J.* **89** 1464, (2005).
- [39] V. I. Novoderezhkin, A. G. Yakovlev, R. van Grondelle, and V.

- A. Shuvalov, J. Phys. Chem. B **108** 7445, (2004).
- [40] T. Förster, Discuss. Faraday Soc **27**, 7 (1959).
- [41] D. I. Dexter, J. Chem. Phys. **21**, 836 (1952).
- [42] A. Redfield, Adv. Magn. Reson. **1**, 1 (1965).
- [43] A. Redfield, IBM J. Res. Dev. **1**, 19 (1957).
- [44] N. Makri and D. E. Makarov, J. Chem. Phys. **102**, 4600 (1995).
- [45] N. Makri and D. E. Makarov, J. Chem. Phys. **102**, 4611 (1995).
- [46] Y. Tanimura, J. Phys. Soc. Jpn **75**, 082001 (2006).
- [47] A. Ishizaki and Y. Tanimura, Jpn **74**, 3131 (2005).
- [48] H.-D. Meyer, U. Manthe, and L. Cederbaum, Chem. Phys. Lett. **165**, 73 (1957).
- [49] M. Beck, A. Jckle, G. Worth, and H.-D. Meyer, Phys. Rep **324**, 1 (2000).
- [50] M. Thoss, H. Wang, and W. H. Miller, J. Chem. Phys. **115**, 2991 (2001).
- [51] S. Jang, Y.-C. Cheng, D. R. Reichman, and J. D. Eaves, J. Chem. Phys. **129**, 101104 (2008).
- [52] S. Jang, J. Chem. Phys. **131**, 164101 (2009).
- [53] S. Jang, J. Chem. Phys. **135**, 034105 (2011).
- [54] A. Nazir, Phys. Rev. Lett. **103**, 146404 (2009).
- [55] D. McCutcheon and A. Nazir, Phys. Rev. B **83**, 165101 (2011).
- [56] A. Kolli, A. Nazir, and A. Olaya-Castro, J. Chem. Phys. **135**, 154112 (2011).
- [57] R. J. Silbey and R. A. Harris, J. Chem. Phys. **80**, 2615 (1984).
- [58] D. P. S. McCutcheon and A. Nazir, J. Chem. Phys. **135**, 114501 (2011).
- [59] D. P. S. McCutcheon, N. S. Dattani, E. M. Gauger, B. W. Lovett, and A. Nazir, Phys. Rev. B **84**, 081305(R) (2011).
- [60] F. A. Pollock, D. P. S. McCutcheon, B. W. Lovett, E. M. Gauger, and A. Nazir, New J. Phys. **15**, 075018 (2013).
- [61] M. Grover and R. J. Silbey, J. Chem. Phys. **54**, 4843 (1971).
- [62] R. Silbey and R. Munn, J. Chem. Phys. **72**, 2763 (1980).
- [63] H.-T. Chang and Y.-C. Cheng, J. Chem. Phys. **137**, 165103 (2012).
- [64] A. Kolli, E. J. O'Reilly, G. D. Scholes, and A. Olaya-Castro, J. Chem. Phys. **137**, 174109 (2012).
- [65] E. N. Zimanyi and R. J. Silbey, Philos. Trans. R. Soc. London, Ser. A **370**, 3620 (2012).
- [66] C. K. Lee, J. Moix, and J. Cao, J. Chem. Phys. **136**, 204120 (2012).
- [67] D. Xu, C. Wang, Y. Zhao, and J. Cao, New J. Phys. **18**, 023003 (2016).
- [68] V. I. Novoderezhkin, E. Romero, J. P. Dekker, and R. van Grondelle, Chem. Phys. Chem **12**: 681 (2011).
- [69] G. Lindblad, Commun. Math. Phys. **48**, 119 (1976).
- [70] M. O. Scully and M. S. Zubairy, *Quantum Optics* (Cambridge University Press, Cambridge, UK, 1997).
- [71] D. Abramavicius and S. Mukamel, J. Chem. Phys. **133**, 184501 (2010).
- [72] M. E. Madjet, A. Abdurahman, and T. Renger, J. Phys. Chem. B **110**, 17268 (2006).
- [73] D. Abramavicius and S. Mukamel, J. Chem. Phys. **133**, 064510 (2010).
- [74] C. Creatore, M. A. Parker, S. Emmott, and A. W. Chin, Phys. Rev. Lett. **111**, 253601 (2013).
- [75] Y. Y. Xu and J. Liu, Phys. Rev. E **90**, 052131 (2014).
- [76] M. Qin, H. Z. Shen and X. X. Yi, J. Chem. Phys. **144**, 125103 (2016).
- [77] J. Wu, F. Liu, Y. Shen, J. Cao, and R. J. Silbey, New J. Phys. **12**, 105012 (2010).
- [78] M. Sarovar, Y.-C. Cheng, and K. B. Whaley, Phys. Rev. E **83**, 011906 (2011).
- [79] X. Chen and R. J. Silbey, J. Chem. Phys. **132**, 204503 (2010).
- [80] F. Fassio, A. Nazir, and A. Olaya-Castro, J. Phys. Chem. Lett. **1**, 2139 (2010).
- [81] J. Struempfer and K. Schulten, J. Chem. Phys. **134**, 095102 (2011).
- [82] C. Olbrich, J. Struempfer, K. Schulten, and U. Kleinekathoefer, J. Phys. Chem. B **115**, 758 (2011).
- [83] Y. Jing, R. Zheng, H.-X. Li, and Q. Shi, J. Phys. Chem. B **116**, 1164 (2012).
- [84] H. Jeffreys and B. S. Jeffreys, *Methods of Mathematical Physics* (Cambridge University Press, Cambridge, 1988).